Prediction of cleavage crack propagation path in a nuclear pressure vessel steel

Xiaoyu Yang, Stephane Marie, Clémentine Jacquemoud, Philippe Bompard

Prediction of cleavage crack propagation path in a nuclear pressure vessel steel

Xiaoyu YANG[1,2], Stéphane MARIE[3], Clémentine JACQUEMOUD[1] and Philippe BOMPARD[2]

[1] CEA, DEN, DM2S, SEMT, LISN, 91191 Gif-sur-Yvette, FR
[2] MSSMat, CNRS, CentraleSupélec, Université Paris-Saclay, 91190 Gif sur Yvette, FR
[3] AREVA, 1 Place Jean Millier, 92400 Courbevoie, FR

ABSTRACT

This paper presents a local stress criterion to predict cleavage crack propagation rate and path in a nuclear vessel steel (16MND5). Experiments are carried out on three different specimen geometries: standard 1T Compact Tensile specimens (CT25), precracked ring specimen (tension & shearing test) and extended Compact Tensile (CT) specimens. Their crack paths are respectively: directionally stable and straight, directionally stable and curved, directionally unstable and deflected. Numerical computations are performed by eXtended Finite Element Method (X-FEM). The combination of the local stress criterion used to determine when the crack propagates to a deterministic direction criterion (based on the classical maximum hoop stress direction) provides a very good prediction for directionally stable crack paths. Furthermore, a probabilistic version of the direction criterion is proposed to predict the directionally unstable crack path. It is then possible to simulate the crack path of the propagation in both extended CT specimens and of conventional CT25 specimens.

This paper aims to predict the dynamic behavior of cleavage cracks in ferritic steel 16MND5. Experiments are carried out on specimens of three different geometries: standard Compact Tension, compression ring and extended Compact Tension. Their crack paths are respectively: directionally stable and straight, directionally stable and curved, directionally unstable and deflected. Numerical computations are performed by eXtended Finite Element Method. A local stress criterion is proposed to predict crack rate. Regarding the direction criterion which is used to predict propagation direction, a deterministic one is enough for directionally stable cracks, but a probabilistic one is necessary for directionally unstable cracks.

Key words: Local approach; Dynamic fracture; Directionally unstable crack path; X-FEM

1 Introduction

The safety demonstration of the PWR (Pressurized Water Reactor) vessel is based on the defect assessment of the vessel subjected to a pressurized thermal shock. In France, this demonstration is limited to the crack initiation: the crack extension is not considered, even if a crack arrest can be demonstrated using a specific criterion.

Therefore, the codified approach to predict the crack arrest in vessel steels, as proposed in the ASME code [1] is not considered for the demonstration performed in France. The ASME method is based on the crack arrest toughness K_{Ia}. This parameter, introduced by Irwin [2], is deduced from a static analysis. This crack arrest criterion is accepted in several countries such as US. It has been verified by the experimental evidence on mock-up tests [3]. However, its physical fundament is considered to be insufficiently understood. That's why a comprehensive work is needed to understand the phenomena involved in the crack arrest process. It can be helpful to consolidate the codified approach and, furthermore, to propose a more physical criterion.

In fact, the standard codified approach based on crack arrest toughness K_{Ia} is questionable for at least two main reasons:

- K_{Ia} is evaluated by static analysis. However, some studies [4,5] highlight the important part played by dynamic effects during the cleavage crack propagation and arrest. The authors point out that there is a difference between the true dynamic Stress Intensity Factor (SIF) and SIF obtained by static analysis. More precisely, it can be summarized as follows:

- Immediately after the crack initiation, the dynamic SIF is smaller than the static SIF, because a part of elastic energy stored in the specimen is converted to kinetic energy after crack initiation.
- Then, the dynamic SIF exceeds gradually the static SIF. That is due to the conversion of kinetic energy to strain energy as the crack speed decreases down to arrest.
- After crack arrest, the dynamic SIF oscillates around the static SIF. This oscillation is strong in the beginning and it damps out with time.

Consequently, in order to depict properly the dynamic crack propagation, arrest and possible reinitiating events in real specimens, some authors find that it is important to take into account the inertial effects [6,7].

Nomenclature	
$a, \dot{a}$	Crack length, crack propagation speed
A, B	Parameters in the critical stress formulation
B_0	Thickness of specimen
da	Increment of crack propagation
dt	Increment of time
D, p	Parameters in Cowper-Symonds law
K_{Ic}	Crack initiation toughness
K_{Ia}	Crack arrest toughness
r_c	Critical distance in RKR model
r_p	Radius of plastic zone at crack tip
T	Temperature
W	Width of specimen
$\dot{\varepsilon}$	Plastic strain rate
ε^p	Equivalent plastic strain at crack tip
$\dot{\varepsilon}^p$	Equivalent plastic strain rate at crack tip
θ, θ_c	Angle to descript the direction of crack propagation
σ_I	Maximum principal stress
σ_{Ic}	Dynamic critical stress in RKR model
σ_{Ic0}	Static critical stress in RKR model
σ_y	Yield stress
$\sigma_{\theta\theta}$	Hoop stress
Principal abbreviations	
CT specimen	Compact Tensile specimen
CT25 (or standard CT25) specimen	CT specimen with a 25 mm thickness
CMOD	Crack Mouth Opening Displacement
fps	Frame per second, unit of framing rate of camera
FE method	Finite Element method
PWR	Pressurized Water Reactor
RKR	Ritchie, Knott and Rice model
SEM	Scanning Electron Microscopy
X-FEM	eXtended Finite Element Method

- The transferability of K_{Ia} from laboratory specimens to structural components is difficult to ensure. In fact, experimental results [3] show that the value of K_{Ia} not only depends on materiel properties but also on specimen geometry. Moreover, the values of K_{Ia} are dispersed especially at high temperature and this dispersion has not been yet explained because the phenomenon of crack arrest is complex due to the dynamic effects.

As an alternative, the local approach provides a better description of the phenomena at the crack tip, and it is more suitable to address transferability issues. The model proposed by Ritchie, Knott and Rice (or RKR model) is one of the first precursory models to predict crack initiation [8]. According to this model, the cleavage crack initiates as soon as the maximum principal stress (σ_I) reaches a critical stress (σ_{IC})

at a critical distance ahead of crack tip (r_c). The distance r_c only depends on the material microstructure. Since, some probabilistic models have been developed such as Beremin model [9]. This type of model is based on a probabilistic description of the phenomena involved in the cleavage fracture initiation.

Inspired by models dedicated to crack initiation, some adaptions are proposed to extend these models to the cleavage crack propagation and arrest. For example, Iung and Pineau [10] evaluate the crack arrest toughness K_{Ia} by applying the Beremin model and RKR model. In order to take into account the dynamic effects, the yield stress (σ_y) in their studies not only depends on the temperature (T), but also on the stain rate ($\dot{\varepsilon}$). Authors find that, contrary to crack initiation, the weakest link theory related to the Beremin model is not appropriate in the case of cleavage crack propagation and arrest.

The local criterion of RKR type to predict crack propagation and arrest is defined by Equation 1: the cleavage crack propagates as soon as the maximum principal stress (σ_I) attains a critical stress (σ_{IC}) at a critical distance ahead of crack tip (r_c), otherwise, the crack arrest occurs.

$$\begin{aligned} f(\sigma) &= \sigma_I(r_c) - \sigma_{IC}(r_c) = 0 \;\; \dot{a} > 0 \\ f(\sigma) &= \sigma_I(r_c) - \sigma_{IC}(r_c) < 0 \;\; \dot{a} = 0 \end{aligned} \qquad \textbf{Equation 1}$$

where $\dot{a}$ is the speed of crack propagation.

Different criteria based on critical stress (σ_{IC}) are developed in the following works:

- Hajjaj et al [12] and Dahl et al [3, 13] propose that the critical stress (σ_{IC}) depends only on the temperature (T) and follows an exponential law similar to the well-known relationship between the cleavage toughness of ferritic low alloy steels and the temperature. This proposition is based on experiments performed on precracked discs subjected to an intense thermal shock (without mechanical load). The material used in their studies is a bainitic steel 18MND5.
- In order to evaluate the impact of local variation in the microstructural resistance, Berdin [14] introduces a Weibull distribution into the critical stress (σ_{IC}) proposed by Hajjaj et al and Dahl et al [12, 13]. The author finds that this local variation in σ_{IC} does not impact the distance of crack propagation, nor the shape of crack front. This result shows that, contrary to crack initiation, the cleavage crack propagation and arrest are related to a collective behavior of grains.
- Meanwhile, Prabel et al [15, 16] and Bousquet et al [17, 18] propose that the critical stress (σ_{IC}) depends on the equivalent plastic strain rate ($\dot{\varepsilon}^p$) at the crack tip (Equation 2). This proposition is inspired by a study of Bouynes [11], and it is based on fifty-three isothermal experiments performed on standard CT25 specimens at four temperatures: -150°C, -125°C, -100°C and -75°C. The material used in their studies is 16MND5 steel.

$$\sigma_{IC} = \sigma_{IC0}\,[\,1 + A.(\dot{\varepsilon}^p)^B\,] \qquad \textbf{Equation 2}$$

Where

r_c	Critical distance ahead of crack tip
σ_{IC}	Dynamic critical stress at the distance r_c
σ_{IC0}	Static critical cleavage stress at the distance r_c
$\dot{\varepsilon}^p$	Equivalent plastic strain rate at the distance r_c
A, B	Coefficients to be identified by experiments

In the criterion proposed by Prabel et al and Bousquet et al (Equation 2), the critical stress is calculated at a distance r_c, which is relevant to the microstructural contributors to cleavage fracture (in particular grain size and carbides repartition). The critical distance r_c is a parameter of the model, and the parameters *A* and *B* are strongly dependent on this distance. Once the critical distance r_c is fixed, the

parameters *A* and *B* of Equation 2 are identified from the calculations of the different experiments on CT25 specimens. In these calculations, the plastic behavior of the material, the viscosity and inertia effects have been considered. The authors show that all test results conduct to a unique relationship between the maximum principal stress and the equivalent plastic strain both calculated at a distance r_c ahead the crack tip.

Note that for the static situation ($\dot{\varepsilon}^p = 0$), the critical stress (noted σ_{IC0}) is close to the cleavage stress at crack initiation.

Bouynes [11] and Bousquet [17] justify the dependency of σ_{IC} on $\dot{\varepsilon}^p$ through the role of ductile ligaments behind the crack tip during cleavage crack propagation. Figure 1 provides a simple illustration to describe the mechanism during the cleavage crack propagation: the ligaments are formed behind the crack tip. Each ligament can be considered as a small tensile specimen that breaks when its plastic strain (ε^p) reaches a critical value, which is supposed to be independent of the strain rate and the temperature [30]. The ligaments are broken beyond a distance *d* from crack tip. During the propagation process, these ligaments act as back springs and resist to the crack opening, therefore they reduce the effective stress close to the crack tip. The SEM observations of the tested specimens confirm the presence these ductile ligaments on the fracture surfaces.

The model supposes that during the propagation process, the same critical stress as the one at initiation should be reached. Since the ligaments are not explicitly modelled in the calculation, their action is represented by an increase of the critical stress: an extra loading is brought to compensate the impact of the ligaments on the crack opening. This corresponds to the second term in the equation 2. Its dependence to the plastic strain rate is directly linked to the viscosity effect on the material behavior. The higher the stain rate is, the harder the material is: the stresses in the ligaments increase with the strain rate. More detailed information about this point can be found in [23].

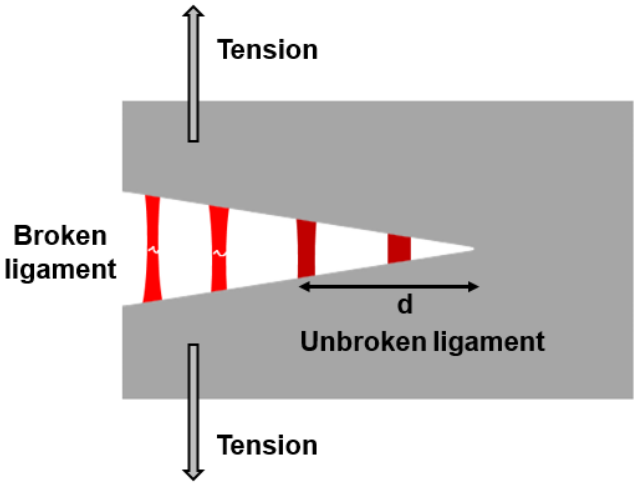

Figure 1: Illustration of ductile ligaments behind the crack tip during cleavage crack propagation and arrest.

The works of Prabel et al [15, 16] and Bousquet et al [17, 18] provide very promising results. However, additional actions are needed to consolidate their proposal:

- The transferability of the criterion to different geometries has to be consolidated;
- As mentioned above, this work is performed to support the consideration of crack arrest in the PWR vessel defect assessment, where the thermal shock is the dominant loading condition. The implementation of the criterion under such loading condition should be defined;
- Finally, the Physical basis of the criterion has to be re-enforced: Bousquet [17] showed that the formalism of the criterion (obtained from F.E. calculation fit) can be derived from a mechanical formulation of the ligaments resistance. However, he made some assumptions which have to be confirmed and quantified more accurately.

The present paper focuses on the first bullet: the transferability issue. Several geometries are considered to get more complex crack path than the straight crack path obtained on conventional CT specimen. The capability of the criterion to predict the crack growth rate and direction will be a key element to verify its validity and transferability. The paper contains six parts:

- In a first part, the material is presented;
- In a second part, the different experiments developed in the frame of this work are detailed;
- Then, the numerical procedure used for the modelling is described;
- Due to the improvement in the numerical procedure, a new identification of the criterion based on the tests on CT25 specimens is carried out;
- Then the modelling of precracked ring specimen (Ø=55mm) subjected to mixed mode loads (tension & shearing) is presented. The deterministic direction criterion proposed by Prabel et al [16], in addition to the equation 2 which only control the crack growth rate, is used;
- Finally, the tests on extended CT specimens, which present unstable deflection during the crack propagation, will be analyzed. In this last part, a probabilistic approach to predict the crack deflection is introduced.

2 Supporting experiments

As mentioned in the introduction, three geometries of specimen are considered in this paper:

- CT25 specimens with reduced thickness. Tests have been performed by Prabel [15] and Bousquet [17] and results are used in this work to fit the criterion by using the new modelling procedure. The crack path is directionally stable, it follows the symmetry plane of the specimen.
- Precracked ring under compression with a machined notch tilted from the loading axis. It is used to make a mixed mode loading condition and produce a non-straight crack growth.
- Extended CT specimen presenting unstable deviation of the crack path from the specimen plane of symmetry.

2.1 Description of material

The ferritic low-alloyed steel studied in this paper is a 16MND5 sampled from a French Pressurized Water Reactor (PWR) vessel. Its chemical composition (Table 1) and its microstructure are close to those of A508 steel. The specimens are oriented to sollicite the crack in the circumferential direction of the vessel.

elements	C	Mn	Si	Ni	Cr	Mo	Cu
%(weight)	0.16	1.35	0.19	0.74	0.18	0.51	0.07

Table 1: Chemical composition of the 16 MND 5 steel used in this study.

The mechanical behavior of 16MND5 at high strain rates and at various temperatures has been identified through dynamic tests on Hopkinson bars [15, 17]. Bousquet [17, 37] proposed to use a Cowper-Symonds law (Equation 3) to represents the viscosity effect. This formulation links the dynamic stress σ_{dyn} to its static value σ_{stat} via an amplification factor depending on the equivalent plastic strain rate $\dot{\varepsilon}^p$.

$$\sigma_{dyn}(\varepsilon^p, \dot{\varepsilon}^p, T) = \sigma_{stat}(\varepsilon^p, T)[1 + \left(\frac{\dot{\varepsilon}^p}{D}\right)^{\frac{1}{p}}] \qquad \textbf{Equation 3}$$

where ε^p is the plastic strain, T is the temperature, σ_{stat} is the static stress, *D* and *p* are constants to be identified by experiments. σ_{stat} has been identified by Chapuliot et al [21]. *D* and *p* have been identified by Bousquet [37] at five different temperatures (Table 2). Bousquet only considers isothermal tests, in order to have the best fit of the experimental data at each temperature, without looking for the consistency of the parameters variation with the temperature. As we consider isothermal tests in this paper, we can use this identification.

T (°C)	D (s^{-1})	p

-150	500 000	4.2
-125	31 000	6
-100	34 000	6.5
-75	16 000	7.2
-50	45 000	5.6

Table 2: Set of parameters (D, p) at five different temperatures (Bousquet, [17]).

In reference [25], a master curve reference temperature T_0 of -121.8°C has been estimated for this material. Except for -50°C where some ductile tearing propagation have been obtained, the failure mode at the other temperatures is a pure cleavage fracture.

2.2 Experimental device

All tests are performed with the same testing device, it is developed specifically for the cleavage crack growth rate measurement, and represented in Figure 2. The cooling of the specimen is performed using a thermal chamber.

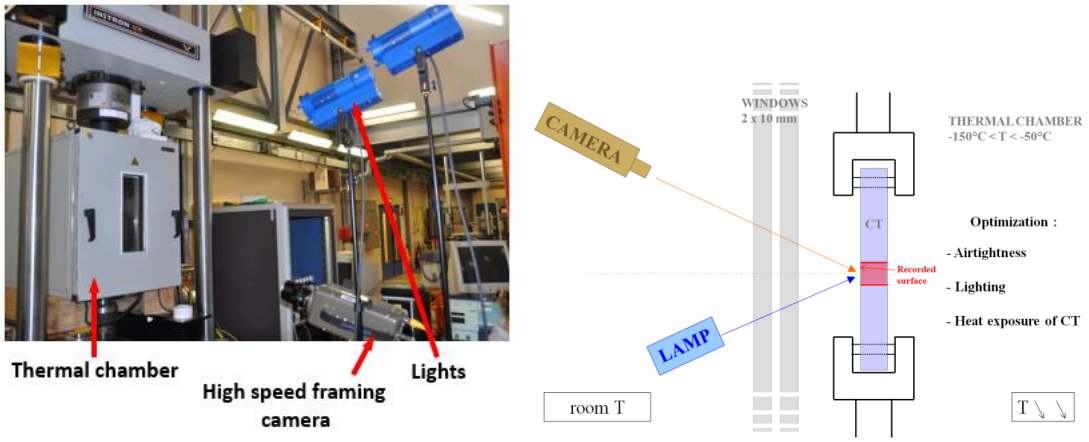

Figure 2 : General view of the testing device.

Usually, the crack propagation is recorded by the crack gages [15, 12]. However, the crack gage technique may be associated to uncertainties linked to early plastic strain debonding or fracture, or to possible multiple crack propagation ahead of the main crack tip. That is why we use an alternative technique to measure crack speed, developed in the frame of the Bouquet PhD [17, 38]. However, there are two main difficulties for using this technique. The first one relies on the fact that cleavage tests are performed in low temperature chambers, leading to the formation of ice on the window and on the specimen. The second difficulty is linked to the very high framing rate required for the camera system since crack speed can reach up to 1000 m/s. It is necessary to record with high accuracy a small region (few centimeters) in a frame rate range from 520 000 frames per second (fps) to 1 100 000 fps.

In order to overcome these difficulties, improvements are first made to the thermal chamber (INSTRON) in order to ensure a perfect isolation and airtightness. In this manner, the formation of ice inside the thermal chamber and on the specimen is avoided. An external lighting is made by two low wattage and low voltage lamps. More details on this device can be found in references [17, 38]. Two image resolutions were used for most of the cases, i.e. 256×32 pixels with 520 000 fps and 128×16 pixels with 1 100 000 fps. At 520 000 fps and 1 100 000 fps, a crack at 600 m/s respectively propagates over 1.15 mm and 0.54 mm between each frame. Around 50 fracture pictures are obtained per test. Figure 3 illustrates the results for a CT25 tested at -150°C.

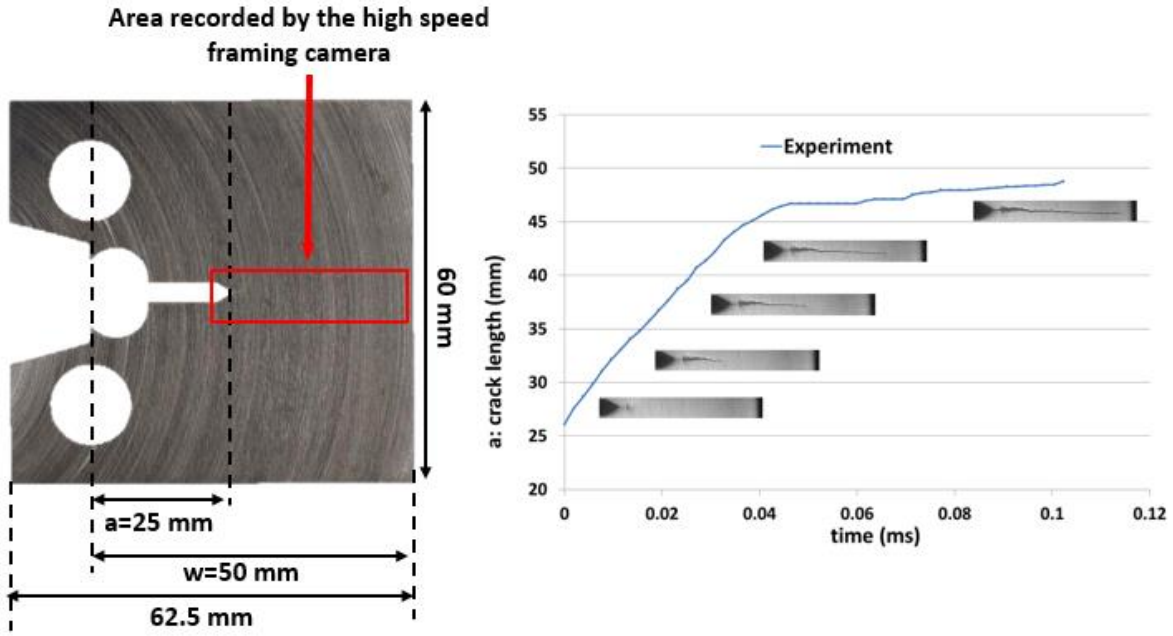

Figure 3: Standard CT25 specimen geometry and crack growth recorded by high speed framing camera at -150°C.

The same instrumentation and testing device are used in the following experiments. Before the test, a fatigue pre-crack of 2.5 mm is realized on each specimen at room temperature according to the conventional procedure. Before the fracture test, the specimen is firstly cooled down to -150°C by nitrogen injection. After the stabilization of temperature, the fracture test begins with a static loading controlled by crosshead displacement. Once the crack initiation is detected, the crosshead displacement is fixed until to the end of test.

During each test, temperature of specimen, mechanical load, Crack Mouth Openning Displacement (CMOD), and all information about crack propagation (crack path, crack speed …) are recorded.

2.3 Tests on CT25 specimens with reduced thickness

CT25 specimens have been tested in the frame of the PhD of Prabel [15], Bousquet [17] and Yang [23]. The geometry is a standard CT25 (considering W = 50 mm), but with a reduced thickness of 10 mm for the major part of them, to avoid a significant tunnel effect during propagation and then to insure that the surface crack growth measurement are applicable to the entire thickness of the specimen. The high speed framing camera is used only during the tests performed by Bousquet and Yang. The crack gages are used during the tests performed by Prabel. However, the consistency of these two types of measurement has been verified by Bousquet [17, 38]. A total of 65 tests is available covering several test temperatures (-150°C, -125°C , -100°C, -75°C and -50°C). Some specimens present a crack arrest with a remaining ligament of few millimeters. The average cleavage crack growth rate is about 600 m/s and the maximum speed attains about 1000 m/s.

2.4 Tests on precracked ring specimens subjected to mixed mode loading

In order to test the transferability of the propagation criterion, a specific specimen was developed by Prabel et al [15, 16] to get a cleavage crack growth under mixed mode condition. The specimen is a precracked ring under compression as represented in Figure 4. It has an inner diameter of 60 mm, an outer diameter of 110 mm, and a thickness of 25 mm. A mechanical notch is machined on the outer diameter, at an angle of 25° from the horizontal plane of symmetry. Thus, under compressive load, the mechanical notch is subjected to both tension (mode I) and shearing (mode II) loads. In the work of Prabel, only one test at -150°C has been performed and the crack propagation has been followed by the crack gages.

In this work, three new tests are carried out at different test temperatures: -150°C, -125°C and -100°C. All information related to crack propagation and arrest (crack path, crack speed ...) are recorded by a high-speed framing camera at 440000 frames/s. Figure 5 shows the crack growth on a specimen tested at -100°C (specimen named 520VV). The crack propagates during about 70 µs with an average speed of about 300 m/s, which is half of the average crack speed on CT25 specimen (600 m/s). After the initiation, the crack direction changes to become parallel to the loading direction. Prabel [16] explains this path by the fact that the crack follows the maximum hoop stress orientation and does not go into the compressive area of the ring, which is close to the inner surface around the symmetry plane of the ring.

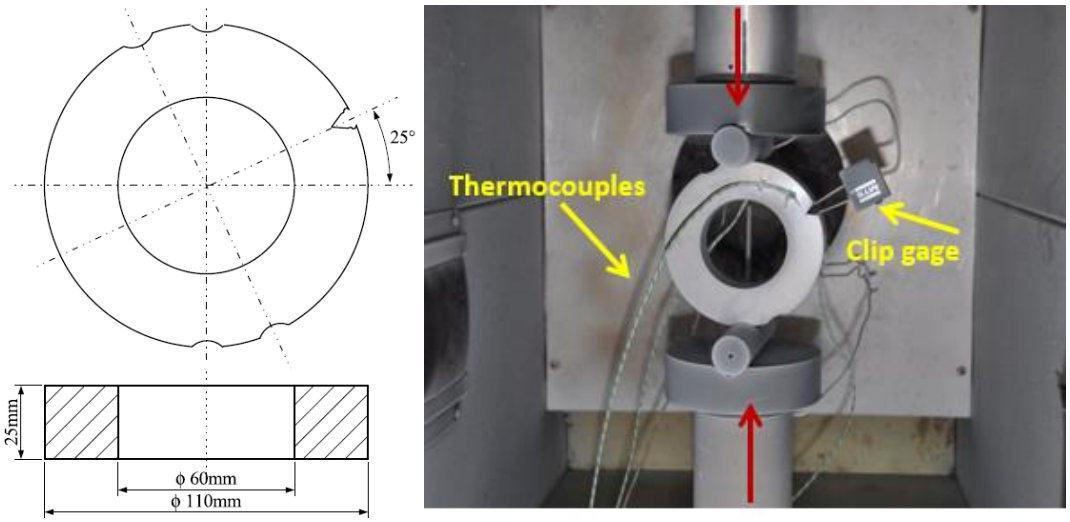

Figure 4: Geometry of precracked ring specimen subjected to mixed mode loading.

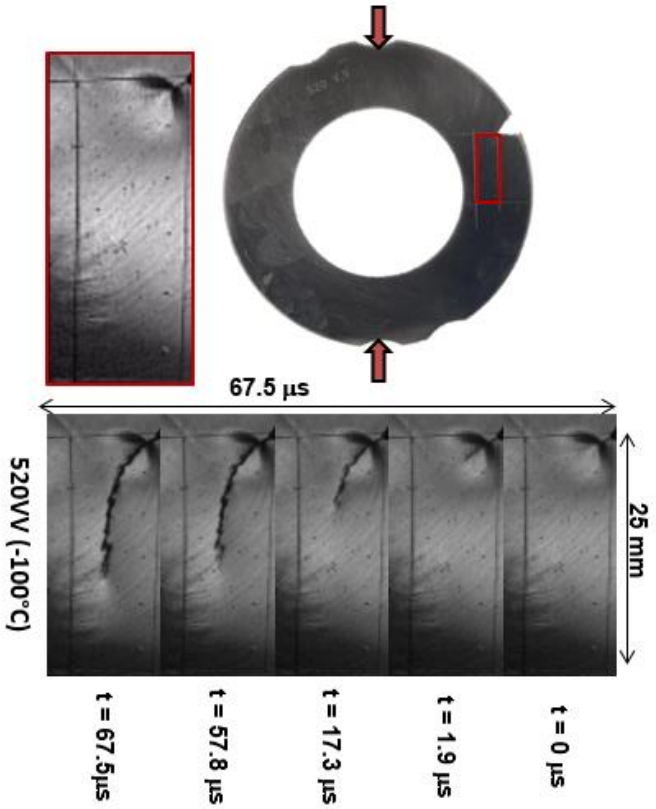

Figure 5: Images of crack propagation recorded by high-speed framing camera for test on 520VV (-100°C).

2.5 Tests on extended CT specimens

The extended CT specimen is used in this work with the goal to get a deflection of the crack path. Compared to the standard CT25 specimen, the extended CT has a double width W The other dimensions are identical. The thickness of the specimens is 25 mm. Bousquet [17] considered in his PhD a thickness of 10 mm, but with this thickness, half of the specimens presented a double crack initiation, which is not analyzed in this work. The increase of thickness improves this situation, only four of the ten tests present this double crack initiation in this work. It is important to point out that we do not note any other influence of the specimen thickness: neither on the stress intensity factor at crack initiation, nor on the deflection of the crack path. However, additional tests are needed to consolidate these observations.

The crack propagation and arrest are recoded by the high speed framing camera at 328500 fps. However, due to the characteristics of camera, only a part of the specimen (≈ 35 mm * 17 mm) corresponding to the red rectangle in Figure 6 is captured. It is not possible to capture the complete crack propagation area with a sufficient framing speed. The choice is made to focus the measurement on the beginning of the test, in order to get an accurate estimation of the initial crack growth rate and of the deflection of the crack path.

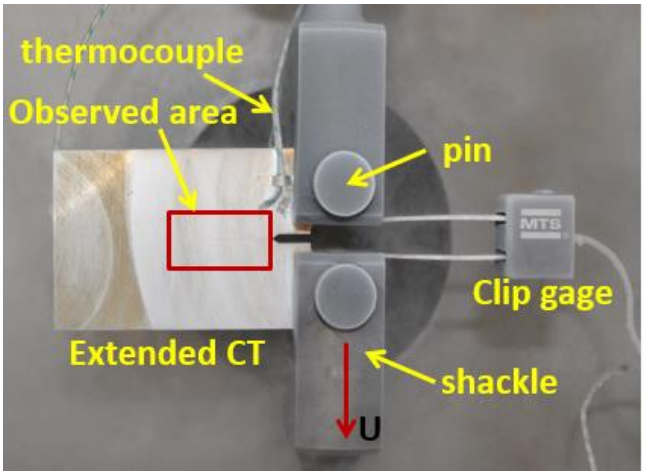

Figure 6: Testing device for extended CT specimen.

We consider here 10 tests presenting only one crack on the specimen. For two of these tests, the load level at crack initiation is very low. In these cases, the crack paths are short and straight, they remain close to the specimen plane of symmetry. For the eight other tests, the load levels at crack initiation are similar (K_J is between 40 MPa.m$^{0.5}$ and 68 MPa.m$^{0.5}$), but the crack paths are very different as presented in Figure 7. For sake of comparison all crack paths are presented deflecting upwards.

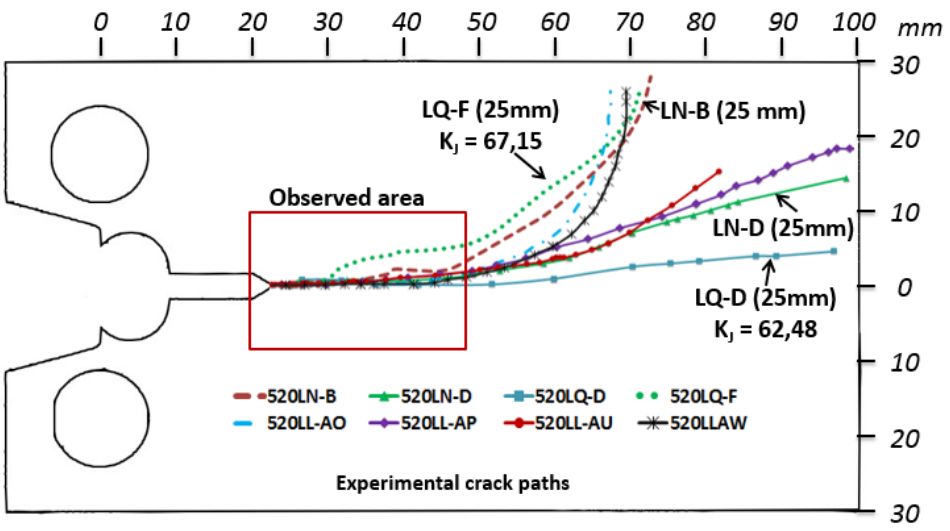

Figure 7: Experimental crack paths on extended CT specimens (K_J is in MPa.m$^{0.5}$).

The initial crack growth and the crack growth rate are presented in Figure 8. The average crack speed is about 600 m/s, which is comparable to the average rate measured on the standard CT specimens.

A specific direction criterion is proposed in section 5.2 to explain and to predict the scatter in the crack paths.

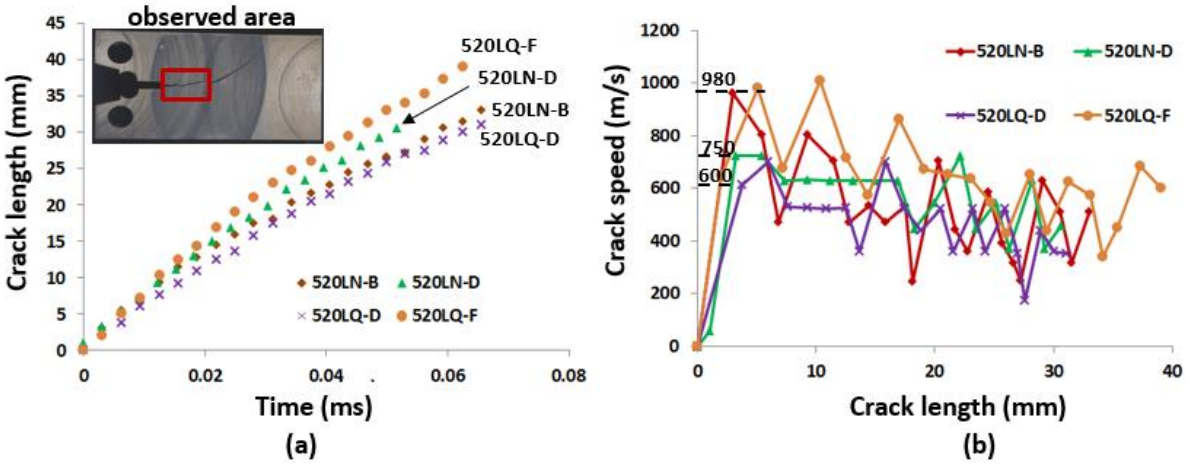

Figure 8: First stages of crack propagation on extended CT specimens, (a) crack growth versus time, (b) crack growth rate versus crack length.

3 Modelling procedure

Before presenting the identification of the criterion and the prediction of the crack propagation, this section presents the numerical tool.

The calculations are performed in 2D by using the plane strain assumption. It should be noticed that the stress singularities induced at the crack tip is very confined, thus the large deformation effects are neglected in the calculations.

3.1 X-FEM

The calculations are performed using the eXtended Finite Element Method (X-FEM) with CAST3M software. The advantage of this method is to integrate directly the degrees of freedom in the element by the following functions:

- a discontinuous function to represent the crack;
- a set of singular functions to capture the displacement field induced by the crack tip.

With this method, the explicit modeling of the crack in the mesh is not necessary, which is a great advantage when the crack path is complex or cannot be anticipated.

The X-FEM has been implemented in Cast3M software by Prabel [15, 26]. The author has used a specific integration strategy to make possible the modeling of a crack propagation with the X-FEM elements in an elastic-plastic media. In fact, the usual technic is based on a conform sub-division of the mesh which implies a projection of the mechanical field. In the case of history-dependent properties, such as the elastic-plastic material, this projection is not compatible with accurate results. The non-conforming method of sub-division initially proposed by Elguedj et al [39] has been used for the integration [26]. The X-FEM elements placed close to the crack have 64 integration points for a more accurate integration. The zone with X-FEM elements is defined a priori and no projection is needed. More details on this point can be found in references [15, 16, 26, 39].

3.2 Explicit formulation for the dynamic calculations

The dynamic calculations are based on a classic explicit formulation. The time approximation used is the one proposed by Newmark [40] with an average acceleration ($\gamma = ½$; $\beta = ¼$), as described by the following equation:

$$u_{n+1} = u_n + \Delta t.\dot{u}_n + \Delta t^2.\left(\frac{1}{2} - \beta\right).\ddot{u}_n + \Delta t^2.\beta.\ddot{u}_{n+1}$$
$$\dot{u}_{n+1} = \dot{u}_n + \Delta t.(1-\gamma).\ddot{u}_n + \Delta t.\gamma.\ddot{u}_{n+1} \qquad \textbf{Equation 4}$$

More details on this point can be found in references [15, 16, 26, 39].

In the modelling, there are two solutions to calculate the crack propagation between two steps:

- Fix the time increment (dt), and then determine the related crack extension (da) with the criterion.
- Work with a constant crack extension (da), and determine the related time increment (dt).

For all solutions, the time increment (dt) should be small enough to capture the dynamic effects, the crack extension (da) should also be small for the accuracy of the calculation. These solutions have been optimized by a sensitivity analysis of the local field in [23]. We have found that:

- When the crack extension (da) is fixed, the value of da = 100 µm is optimal. The time increment deduced from the application of the propagation criterion should be lower than 5.10^{-6} s.
- When the time increment is fixed, the value of dt = $0.5.10^{-6}$ s is optimal. The crack extension (da) should be lower than 300 µm.

These two solutions are proved to be equivalent because they give the same local mechanical fields during the propagation process [23].

It should be noted that these parameters are optimized for mesh sizes between 50 x 50 µm² and 100 x 100 µm².

3.3 Crack propagation criterion

The propagation criterion is based on the maximum principal stress (σ_I) and the equivalent plastic strain rate ($\dot{\varepsilon}^p$) calculated at the distance r_c ahead the crack tip. This distance r_c is a parameter of the model and could be defined arbitrarily, but it should be relevant of the microstructural feature of the cleavage

fracture initiators. The characteristic size usually considered is the average grain size or the average distance between carbides. For the materials similar to the steel considered in this study such as A508, 18MND5 this characteristic size is taken between 10 and 100 µm [10, 11, 12, 13, 15]. The critical distance r_c is fixed to 100 µm for all the calculations in this work, Note that the r_c value is linked to the model's parameters (the critical stress and the equivalent plastic strain rate): a change in the r_c choice implies a new identification of theses parameters.

In order to limit the impact of local numerical variations of the mechanical fields, the maximum principal stress (σ_I) and the equivalent plastic strain rate ($\dot{\varepsilon}^p$) are averaged in an area of 50 x 50 µm², centered at the distance r_c from the crack tip. However, they are calculated at one integration point in the works of Bouquet and Prabel. The numerical results are more stable with the method of this work, that's why a new criterion identification is developed in section 5.

In the criterion identification, the experimental crack growth deduced from the crack gages or the high speed camera is used to pilot the crack growth in the calculation. At each crack extension, the local maximum principal stress σ_I and the equivalent plastic strain rate $\dot{\varepsilon}_p$ are estimated by the method described in the previous paragraph.

In predictive simulations, the crack extension increment (da) is fixed at 100µm, and we look for the time increment (dt). More precisely, at the time t_i, the crack length is a_i, and for the next step, $a_{i+1} = a_i + 100$ µm, the time t_{i+1} is determined through a dichotomy algorithm. The algorithm is considered converged when the condition in Equation 5 is fulfilled.

$$\frac{\left|\sigma_I(t_{i+1}) - \sigma_{Ic}\left(\dot{\varepsilon}_p(t_{i+1})\right)\right|}{\sigma_I(t_{i+1}) + \sigma_{Ic}\left(\dot{\varepsilon}_p(t_{i+1})\right)} < tolerance \qquad \text{Equation 5}$$

where $\sigma_{Ic}\left(\dot{\varepsilon}_p(t_{i+1})\right)$ is the propagation criterion given in equation 2. The tolerance is fixed at 5%, which insures a good compromise between the accuracy of the predictions and the convergence speed of the algorithm.

If the time increment exceeds 5 µs, it is considered that the crack extension is not possible. In this case $a_{i+1} = a_i$ and $t_{i+1} = t_i + 5$µs. After several time increments without crack extension, the crack is considered definitely arrested.

More details on the numerical procedure are provided in reference [23].

3.4 Crack direction criterion

When the crack direction is not imposed in the modeling, the propagation criterion described in the previous paragraph shall be combined to a direction criterion to determine the direction of the next crack extension.

As done by Prabel [16], we use the classical criterion based on the maximum hoop stress: once the critical stress is reached, the hoop stress is calculated at the distance r_c around the crack tip, using the same procedure than for the maximum principal stress (paragraph 4.3). The maximum value defines the direction of the next crack extension.

4 Propagation criterion identification on CT25 specimens

As mentioned in the previous section, the estimation of the stresses and the strain rate at the distance r_c from the crack tip has been improved since the Prabel and Bousquet works. In order to limit the local numerical variations due to the interpolation of mechanical fields, a local average value is considered. For the criterion identification, the crack extension is directly controlled by the experimental crack propagation in 2D simulations.

53 CT25 tests have been modelled corresponding to four different temperatures: -75°C, -100°C, -125°C and -150°C. Thus, the main mechanism of crack propagation is the cleavage for all tests.

The mesh of a CT25 specimen is shown in Figure 9. Only one half of the specimen is modelled because of the symmetry. It contains two parts:

- The part along the crack path (elements in red color in Figure 9) where the elements are linear X-FEM elements, each one containing 64 Gauss points. The mesh size of this area is $(50 \times 50)\mu m^2$;
- The rest of specimen (elements in blue color in Figure 9) where the elements are standard linear elements, each one contains only 4 Gauss points.

Moreover, one elastic rod is modelled to simulate the stiffness of the testing machine and ¼ of pin is modelled to apply the mechanical load. The stiffness has been estimated from the experimental load-jack displacement curve [15, 23].

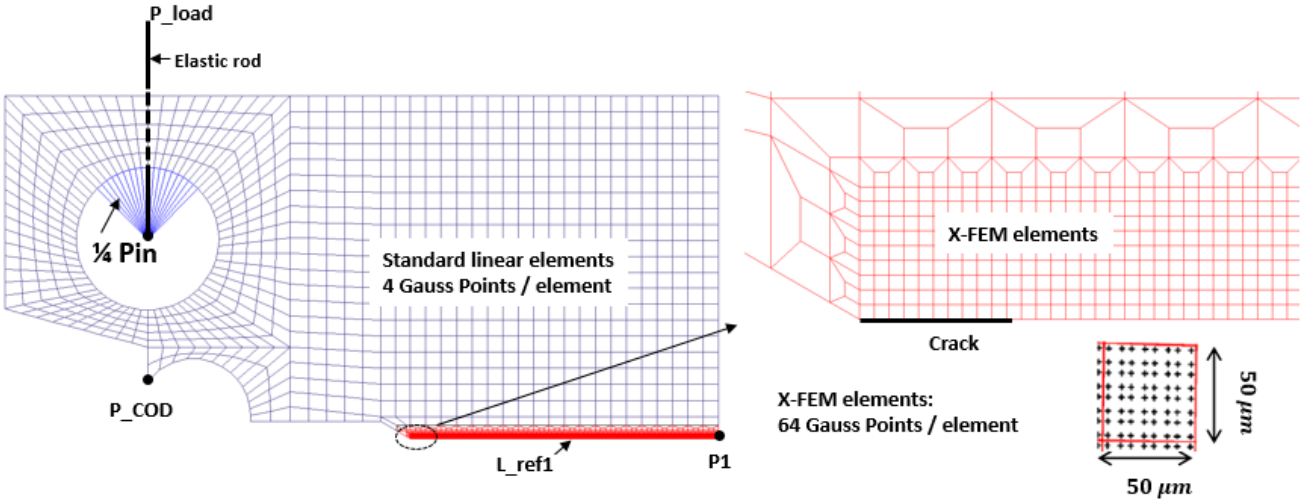

Figure 9: 2D mesh of standard CT25 specimen.

The modelling of each test is performed in two steps:

- The first step corresponds to the initial mechanical loading of the specimen. It aims to obtain experimental conditions at crack initiation. This stage is carried out in static conditions, the material behavior being elastic-plastic. The end of this step is reached when the numerical CMOD attains the experimental one at crack initiation.
- The second step is the crack propagation. During this step the experimental crack propagation is imposed as an evolutive boundary condition. At each crack extension, the maximum principal stress and the equivalent plastic strain rate are calculated on the symmetry plane in the ligament at a distance r_c = 100 µm from the crack tip. The calculation in this step takes into account inertia and viscosity effects.

Variations of the maximum principal stress σ_I with the equivalent plastic strain rate $\dot{\varepsilon}^p$, obtained for the simulations of 53 tests at four different temperatures (from -150°C to -75°C), are plotted in Figure 10.

.

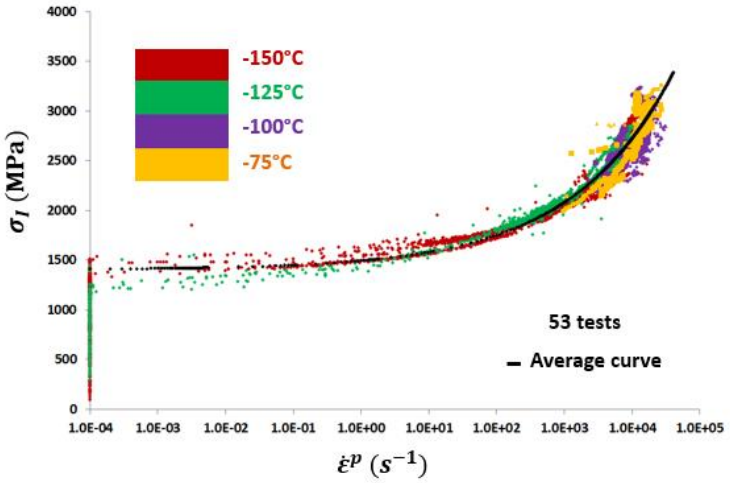

Figure 10: Identification of crack propagation criterion (RKR type), based on 53 isothermal tension tests on standard CT25 specimens at four different temperatures.

We note from Figure 10 that:

- At low equivalent plastic strain rate ($\dot{\varepsilon}^p \leq 1$), the maximum principal stress (σ_I) is nearly constant and close to the critical cleavage stress identified at crack initiation [31, 34].
- Then, σ_I increases with $\dot{\varepsilon}^p$, especially at high equivalent plastic strain rates ($\dot{\varepsilon}^p > 10E^4\ s^{-1}$) σ_I increases exponentially with $\dot{\varepsilon}^p$ as found by Prabel [15, 16] and Bousquet [17].
- Each color represents the results obtained at a given temperature. No significant effect of the temperature is then observed. However, this result should not be generalized, as only one material has been analysed. Furthermore, the range of temperature in this study is between -150°C and -75°C, which corresponds to the lower part of brittle-to-ductile transition curve. A more important influence of the temperature on the criterion cannot be excluded for upper part of brittle-to-ductile transition curve.
- An average trend curve (in black color) is fitted in Figure 10 according to the equation 2 formulation. Its analytical formulation is Equation 6 :

$$\sigma_{IC}(r_c) = \sigma_{IC0}\,[\,1 + 0.065(\dot{\varepsilon}^p\,(r_c))^{0.29}] \qquad \textbf{Equation 6}$$
$$\text{With } r_c = 100\ \mu m,\ \sigma_{IC0} = 1400\ MPa$$

Compared to the previous identification made by Prabel and Bousquet, the use of average local field values leads to a reduced scatter in the calculation results and provides a more reliable estimation of the model parameters. As mentioned in [15], the value of σ_{IC0} is close to usual values identified for the critical cleavage stress.

Note that 3D calculations of the 53 tests have also been performed and have provided results close to those presented in Figure 10, which consolidate the criterion identification given in equation 6.

5 Prediction of crack propagation and path

5.1 Modelling of tests on precracked rings subjected to mixed mode loading

In this section, a first validation of the criterion is performed by the modelling of the precracked rings submitted to a mixed mode loading (I+II) condition. Here, both the propagation criterion (equation 6) and the direction criterion based on the maximum hoop stress, as explained in sections 3.3and3.4, are used.

The calculations are performed in 2D, considering the plane strain condition. No large deformation or large displacement assumption are considered in these calculations. As 2D mesh of CT25, the mesh of precracked ring specimen contains also two parts (Figure 12). One part (in red color) is modeled with

X-FEM elements, where the crack can propagate. The element size in this area is $(50 \times 50)\mu m^2$. The rest of the mesh (in green color) is modeled with standard linear elements.

As for the identification of the criterion, the calculation is performed into two steps: the first one corresponds to the static specimen loading up to the crack initiation defined from the experimental CMOD and the second step is the propagation step.

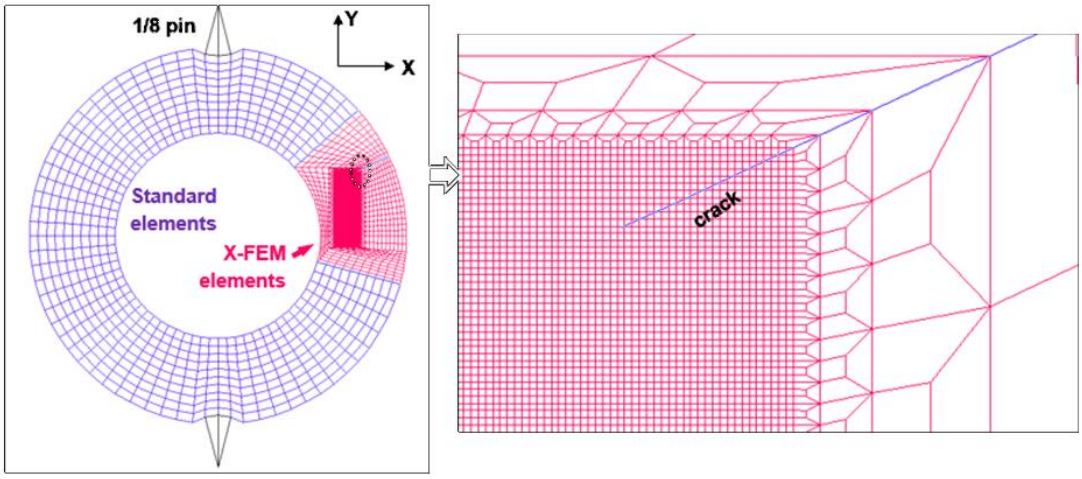

Figure 11: Mesh of cracked ring subjected to mixed mode loading with a zoom on the mesh close to the initial crack tip.

The results of numerical prediction of the tests performed at three different temperatures (-150°C, -125°C, -100°C) are presented from Figure 12 to Figure 14. They are compared to experimental crack path and crack propagation. A good agreement between numerical results and experimental results is found, which confirms the good transferability of the local criterion from a standard specimen geometry (CT25) to a more complex configuration. Detailed information about section aspect can be found in [20, 23].

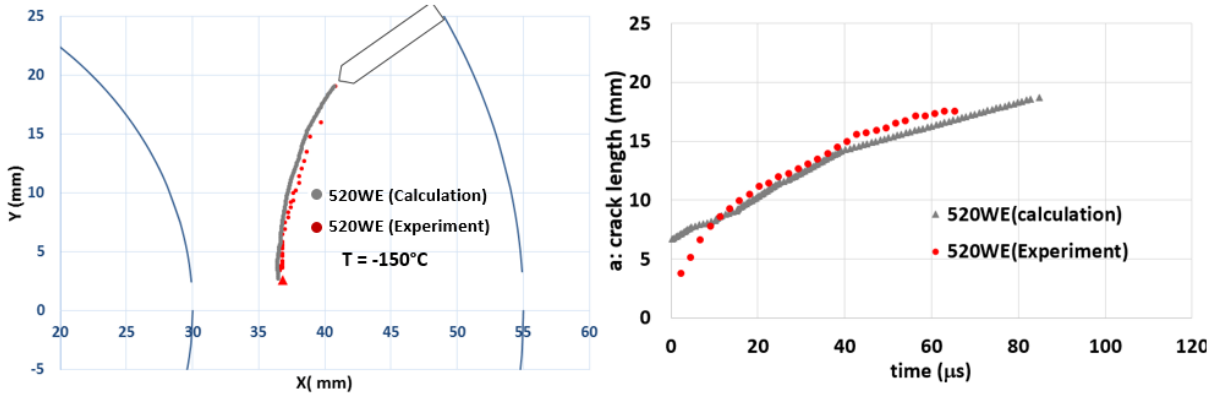

Figure 12: Crack path and crack propagation on a precracked ring subjected to mixed mode loading. Comparison between simulations and experiments for the test on 520WE specimen (-150°C).

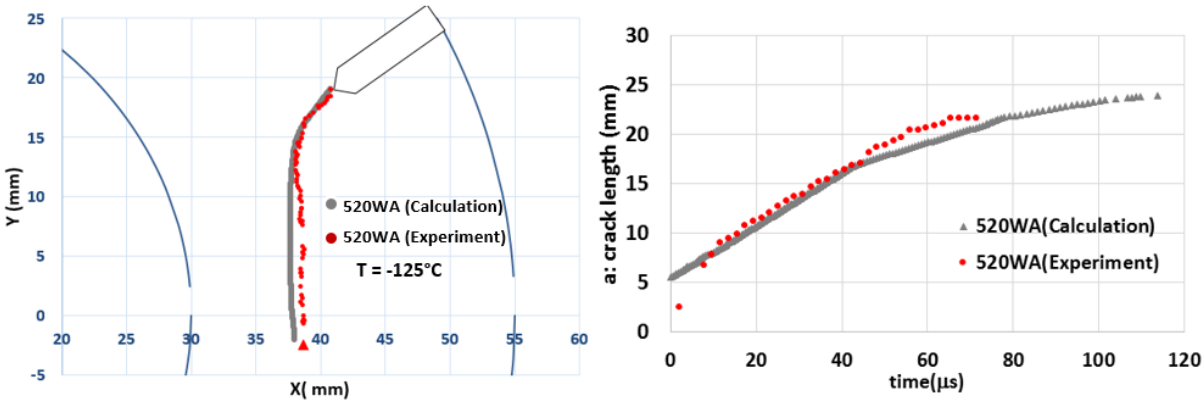

Figure 13: Crack path and crack propagation on a precracked ring subjected to mixed mode loading. Comparison between simulations and experiments for test on the 520WA specimen (-125°C).

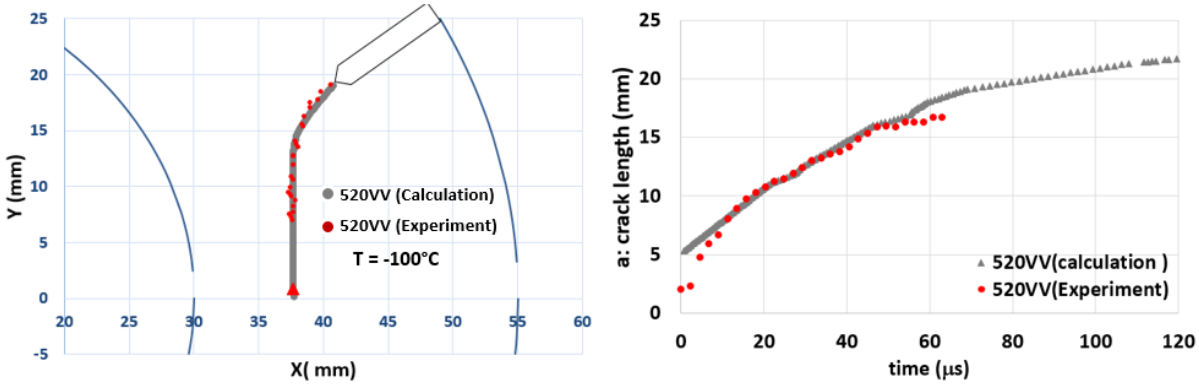

Figure 14: Crack path and crack propagation on a precracked ring subjected to mixed mode loading. Comparison between simulations and experiments for the test on 520VV specimen (-100°C).

5.2 Modelling of tests on extended CT specimens

In order to complete the verification of the transferability of the propagation criterion, this section presents the calculations of the tests on extended CT specimens. As shown in section 3.3, the crack paths are deflected from the symmetry plane of the specimen, and present an important scatter.

The same procedure as for the precracked ring is used, combining the propagation criterion of equation 6 and the direction criterion based on the maximum hoop stress. However, the predicted crack propagation remain straight in the symmetry plane of the specimen. It shows that the direction criterion as proposed in section 4.5 is not able to catch the direction instability of the crack path on extended CT.

5.2.1 Origins of observed crack deflection

The deflection of the crack path is usually observed on Double Cantilever Beam (DCB) specimens. In order to simulate this phenomenon, Sumi [27] introduces, at crack initiation, a small perturbation in the direction of crack propagation. More precisely, the crack propagates at a slight angle between 3° and 8° from the specimen plane of symmetry. With this strategy, the crack leaves gradually the symmetry plane, and the crack path becomes curved as observed during experiment. The author associates this perturbation of the crack initiation to the local microstructural imperfections, such as the orientation of grains.

The mechanisms during crack propagation in both standard CT25 and extended CT are similar. They are investigated from the cross section analyses carried out on a standard CT25. The detailed results of this investigation are presented in reference [23]. Only the relevant conclusion is presented here to justify the new proposition to predict the crack path deflection.

As presented in Figure 15, a cross section in the middle of CT25 (behind the current main crack front) is analyzed by SEM. The crack speed at this location is about 600 m/s. We note the presence of numerous micro-cracks around the main crack, as usually observed for cleavage fracture. According to the fracture micro-mechanism of cleavage, these micro-cracks are developed inside the plastic zone around the propagating crack tip.

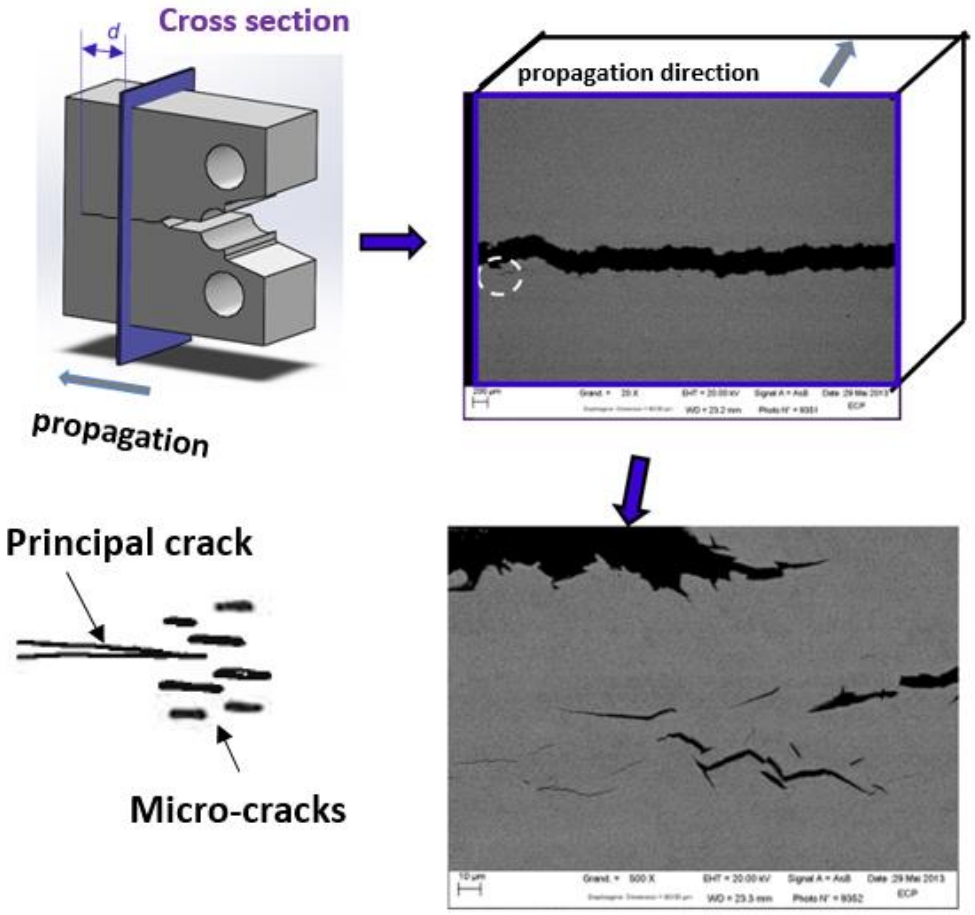

Figure 15: SEM analysis on the cross-section of a standard CT25 (520HO3A, -150°C).

Pictures recorded by the high-speed framing camera during the crack propagation on an extended CT tested at -150°C (520LN-B) are presented in Figure 16. We note that at crack initiation two cracks (1a, 1b) appear simultaneously ahead of the crack tip. Then, the branch 1b stops and the branch 1a continues to propagate. Two new cracks appear ahead of branch 1a, named respectively 2a and 2b. After, the branch 2a stops, and the branch 2b continues to propagate. From this example, we can propose the following scenario of crack propagation:

- Serval micro cracks initiate simultaneously ahead of main crack tip in the most loaded area.
- The main crack propagates to join one or more additional micro cracks ahead of the crack tip.
- Therefore, the direction of crack propagation is random for each step. These local perturbations may be related to the microstructure of material (orientation and size of bainitic lathes, prior gamma grains …).

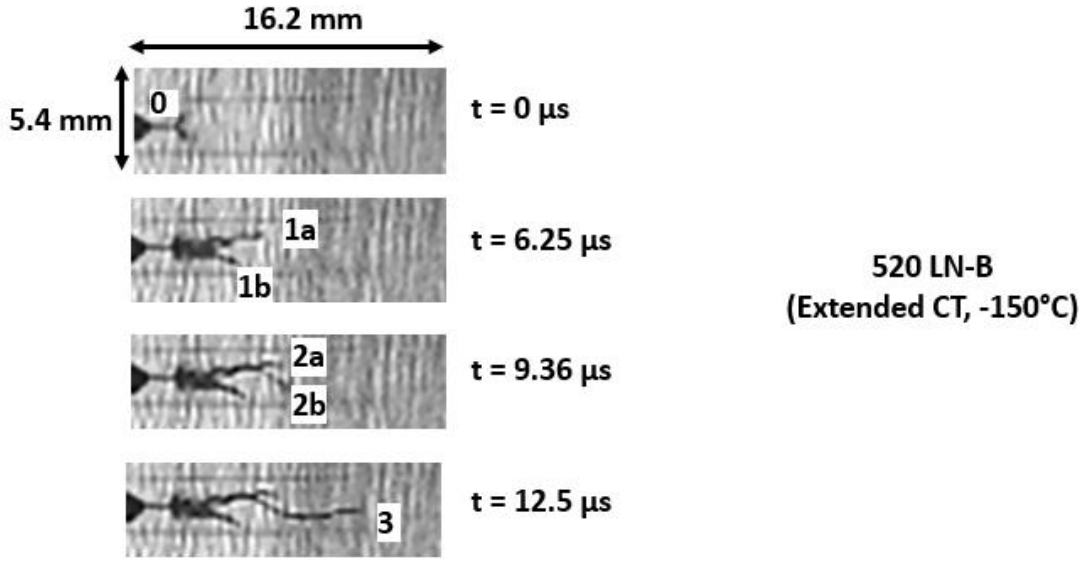

Figure 16: Consecutive pictures recorded by the high-speed camera on an extended CT tested at -150°C. The crack path is 0→1a→2b→3.

More precisely, the propagation direction is not a deterministic phenomenon but obeys a probabilistic mechanism related to the microstructure of material.

The mechanism proposed is illustrated in Figure 17:

- Several micro-cracks initiate inside the plastic zone (characterized by its radius r_p) in the vicinity of main crack tip.
- The main crack can propagate and join these micro-cracks only in the area where the opening stress level is high enough for propagation (characterized by the angular range α in Figure 17).
- The main crack follows a random direction within this highly stressed angular domain, to join one of the existing micro-cracks in this area.

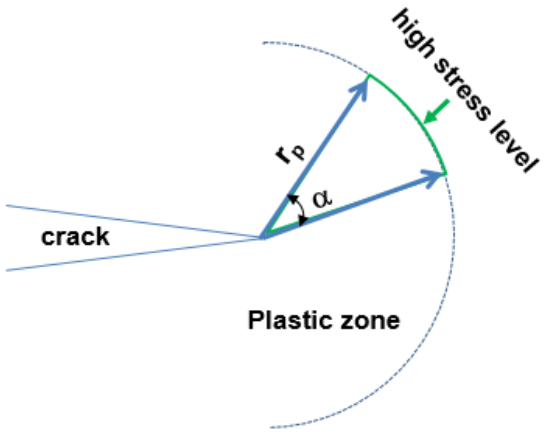

Figure 17: Direction of crack propagation: the crack propagated towards an area where the opening stress level is high.

In summary, there are two necessary conditions to get an instable deflection path during the crack propagation:

- Local perturbations of the crack extension process, which can be created by the micro-cracks mechanism mentioned above.
- A specimen geometry promoting instable crack path such as the DCB specimen.

Some authors, such as Chen and Dillar [28] and Becker at al [29], propose a criterion based on the T stress to judge the crack stability in a given geometry. They show that if T stress < 0, the crack path is directionally stable, otherwise, the crack is directionally unstable and the crack deflection can occur. This paper has not yet evaluated the T stress value of the extended CT, however the T stress of the standard CT specimen is already proved positive [13, 32], and the crack path on standard CT25 is directionally stable. Some authors, such as Leguillon [35], Sapora and al [36], propose a fracture criterion based on the average circumferential stress at a finite distance from the crack tip. According to this type of criterion, there is a positive T stress threshold, above which the crack becomes directionally unstable, and the crack path becomes deflected as it is observed in extended CT specimen. The important role of an important positive T stress on the crack path is also highlighted by Sumi et al [41]. From the expression of the stress field ahead of the crack tip considering the higher-order stress field parameters (T stress and coefficients related to the $x^{0.5}$ term), the authors derive the shape parameters of the crack path and confirm the role of the positive T stress in the curvature of the crack path.

5.2.2 Proposition of a new probabilistic directional criterion

The numerical computations are performed by using the same modelling assumptions and procedure as in the previous calculations.

The mesh of extended CT contains also two parts as shown in Figure 18: one part (in red color) is modeled with X-FEM elements, on which the crack can propagate, and the other part (in green color) is modeled with standard linear elements.

Since the crack path is unknown in this section, the area of crack propagation (X-FEM zone) is modeled large enough to limit the influence of mesh on crack path. However, the increase of the X-FEM zone leads to a significant increase of Gauss point number in the model, and the simulations become very time-consuming. In order to lighten these simulations, two simplifications are used:

- Increase the element size to $(200 \times 200)\mu m^2$. In this way, the size of the element appears very coarse but it must be recalled that:
    - The X-FEM element includes in their formulation all degrees of freedom corresponding to the elastic singular displacement field, which increases significantly the local field description compared to the standard linear element.
    - The X-FEM element has 64 integration points compared to 4 in standard linear element, which also increases the accuracy of the stress field.

  Thanks to these two points, the mesh size remains fine enough for the purpose of the calculation.
- Limitation of the X-FEM area. Since most of experimental crack paths do not cross the specimens completely, we focus only on the first 35 mm of crack propagation (red area in Figure 18). This choice may affect the crack path when the crack approaches the interface between X-FEM and standard FEM areas.

However, the objective of this study is to investigate the possibility to predict the instable deflection process. If this point is conclusive, we will investigate modelling the crack deflection more accurately, with more fine X-FEM elements and larger X-FEM area.

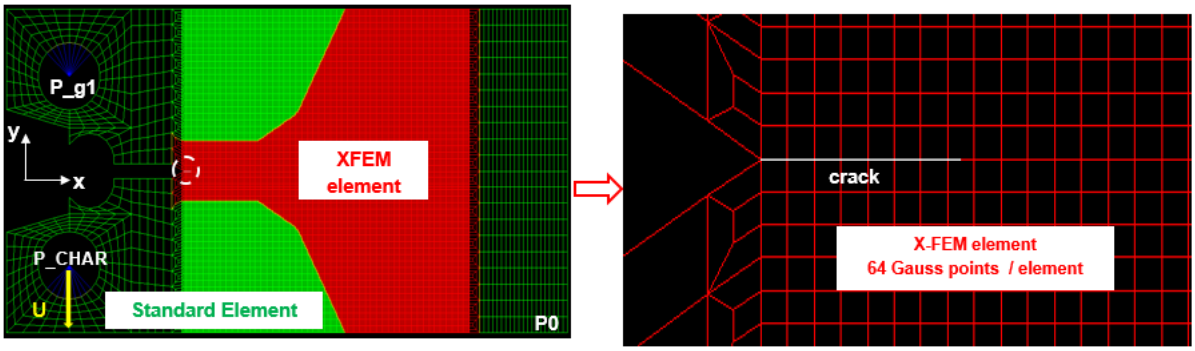

Figure 18: 2D mesh of the extended CT specimen.

The boundary conditions and the modelling sequences are the same as those in the numerical computations of standard CT25.

As explained in section 7.1, the crack path deflections are firstly related to the local perturbation on the crack propagation direction due to micro-cracks at the crack tip. In order to reproduce the local perturbation numerically, we propose to use a probabilistic approach in the calculation of the direction of crack propagation. In the modelling process described in sections 4.4 and 4.5, this new direction criterion replaces the deterministic maximum hoop stress criterion. The rest of the modeling algorithm remains unchanged.

The procedure for this probabilistic direction criterion is as follows:

- At each step of crack propagation, we calculate the maximum hoop stress $\sigma_{\theta\theta}$ on a half circle with a radium of 100 µm (critical distance in the local criterion of RKR type) ahead of the crack tip. We assume that the crack can propagate randomly in an angular domain Δα () of high stress level, where the hoop stress $\sigma_{\theta\theta}$ exceeds 90% of the maximum value $\sigma_{\theta\theta\,max}$.

$$\Delta\alpha = \{\theta: \quad \sigma_{\theta\theta}(r_c, \theta) \geq 0.9\, \sigma_{\theta\theta\,max}\} \qquad \textbf{Equation 7}$$

where $\sigma_{\theta\theta\,max} = \max[\sigma_{\theta\theta}(r_c, \theta)]; r_c = 100\,\mu m; \theta \in [-90°; 90]$

  It should be noted that the threshold value ($0.9\,\sigma_{\theta\theta\,max}$) is a pragmatic choice, and its micromechanical justification will be investigated in the future.

- Within the angular domain Δα, the direction (θ_c) of crack propagation is chosen randomly. In this preliminary study, we assume that the micro-cracks' distribution is uniform, thus, the direction of propagation is chosen randomly according to a uniform law.

5.2.3 Numerical results on extended CT

In order to evaluate the influence of toughness at crack initiation (K_J) on the crack path, two different levels of K_J are considered in this paper: K_J = 40.1 MPa√m and 68.23 MPa√m. In order to take into account the probabilistic character in the direction of crack propagation, 10 simulations are carried out for each K_J level. All simulated tests are performed at -150°C. Numerical crack paths, predicted using the probabilistic approach on the direction of crack propagation are presented in Figure 19 and Figure 20 for two different levels of K_J at crack initiation.

It should be noted that, the crack can deflect upwards or downwards randomly during simulations but they are presented on the same side (upwards) to ease the comparison. We note that:

- For high levels of toughness at crack initiation (K_J) (Figure 20) all numerical crack paths are deflected as it was observed during experiments.
- For low levels of toughness at crack initiation (K_J) (Figure 19) numerical crack arrest occurs earlier for some simulations whereas other predicted cracks are longer and deflected. It is qualitatively representative of the available experimental results: test (520LQ-B specimen) presents an early crack arrest and test (520LL-AW specimen) has a longer deflected crack path.
- For a given toughness at crack initiation (K_J) (both in Figure 19 and Figure 20), an important scatter in predicted crack paths is observed, which seems to increase with K_J at crack initiation. Nevertheless, the number of available experimental results is not sufficient to confirm this observation.

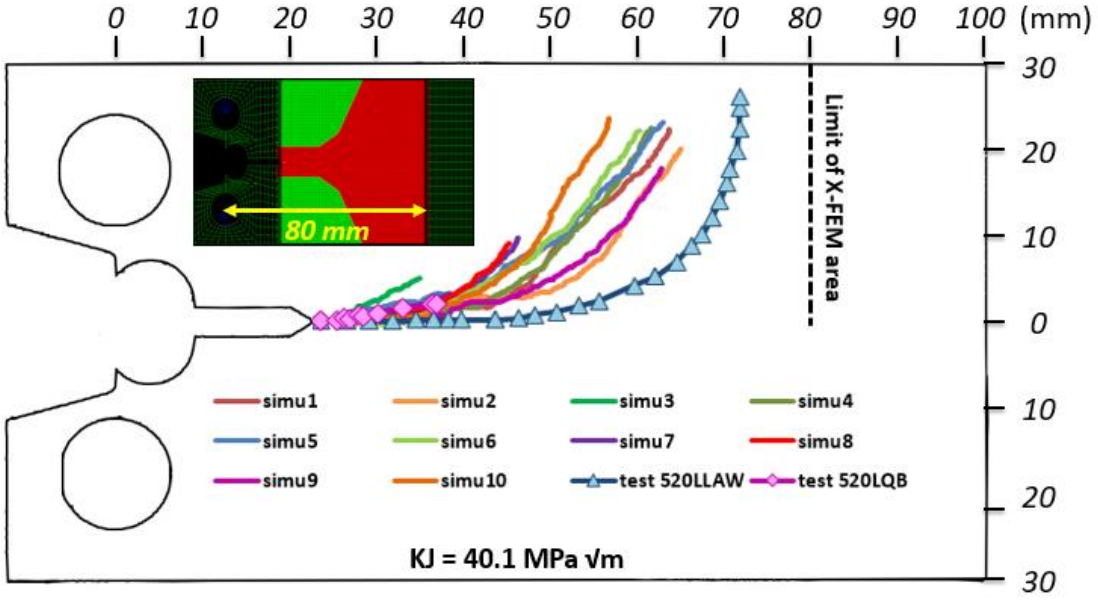

Figure 19: Comparison between experimental crack paths and predicted crack paths on extended CT, with the probabilistic criterion on the crack propagation direction, with K_J = 40 MPa√m at crack initiation.

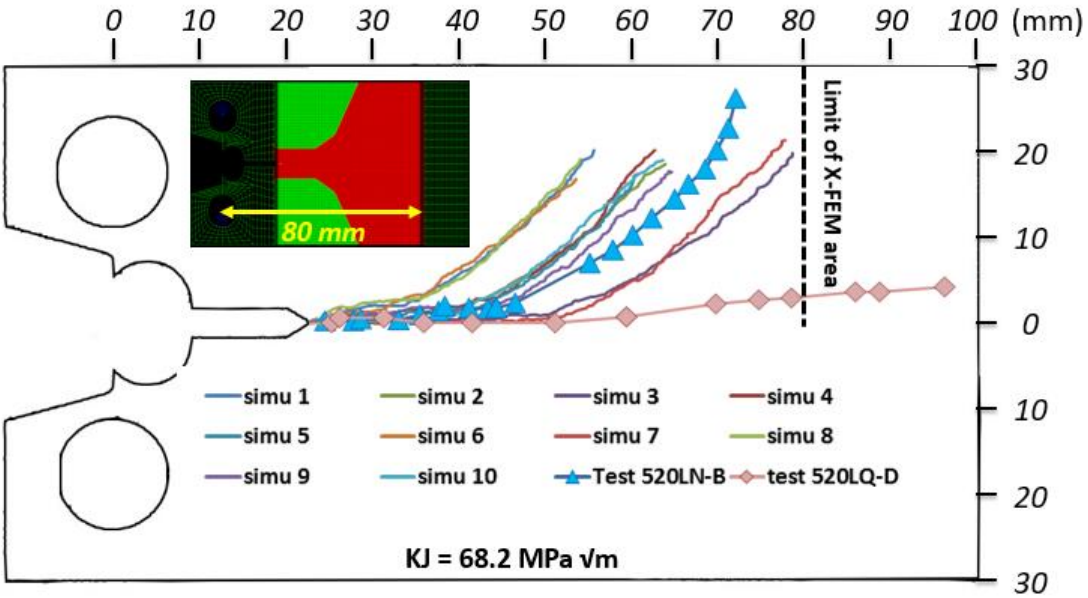

Figure 20: Comparison between experimental crack paths and predicted crack paths on extended CT, with the probabilistic criterion on the crack propagation direction, with K_J = 68 MPa√m at crack initiation.

Numerical crack growth lengths a(t), for two levels of K_J at crack initiation, are plotted in Figure 21 and compared to experiments. It should be noted that the experimental crack growth is measured in a restricted area (showed in section 3.3), that is why the experimental a(t) does not correspond to the end of the test. We note that:

- For high toughness level at crack initiation (K_J), we have four available experimental a(t) curves : 520LN-D, 520LQ-D, 520LQ-F and 520LN-B, K_J of these tests is between 62.5 and 68.2 MPa√m.
- For low toughness level at crack initiation (K_J), we have only one experimental a(t) curve : 520LQ-B.
- According to the numerical results, the crack speed is higher with high level of K_J, which is in close agreement with experiments.

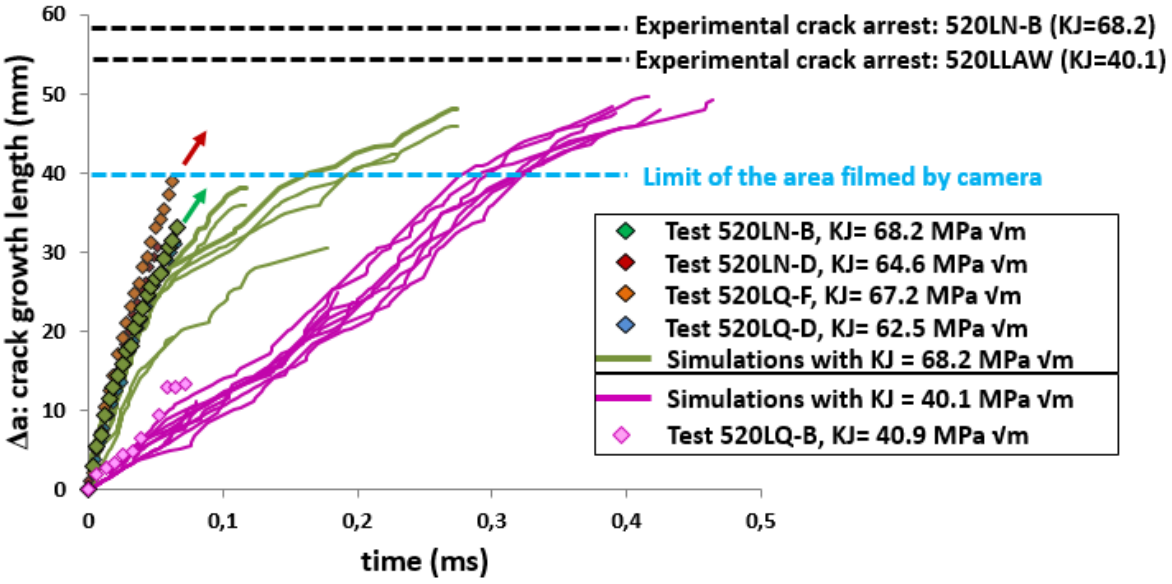

Figure 21: Numerical crack growths for two sets of simulations with different K_J at crack initiation.

However, compared to the experimental crack paths, the predicted crack paths seem to deflect earlier. Two issues can be investigated to improve numerical computations on extended CT:

- First, in the criterion to predict the direction of propagation (5.3.2), the threshold value ($0.9\ \sigma_{\theta\theta\ max}$) is a pragmatic choice, a more physical threshold should be applied. The analysis of defect size ahead of the crack tip could be a starting point of the investigation, because a big defect needs a lower stress to generate fracture than a smaller one.
- Then, the mesh of extended CT should be improved. The mesh used in this paper may have some impact on the crack path because the area for crack propagation (X-FEM zone) is limited to only a part of the specimen.

The probabilistic criterion on the crack propagation direction seems efficient to predict the instable deflection of the crack path on extended CT. In the next section, we will verify the validity of this probabilistic criterion on the prediction of the stable crack path on standard CT25.

5.2.4 Numerical results on standard CT25

The mesh of standard CT25 in this section is obtained by cutting the mesh of extended CT specimens (presented on Figure 18) to a width of W = 50 mm. The procedure of numerical computation is the same as in section 5.2.3.

In this paper, six simulations are performed on one test (520RX-I, -150°C). The six predicted crack paths are plotted in Figure 22. We note that:

- The numerical crack paths are globally straight (less than 3mm aside the symmetry line, Figure 22 (a)), which is consistent with the observations during experiments.
- Local variations on numerical crack paths are observed (Figure 22 (b)), which is in close agreement with experiments.
- The crack arrest lengths are still well predicted: the numerical computations do not predict a complete failure of the specimen, as it is observed during experiment (520RX-I), although the unbroken ligament is less than 1 mm.

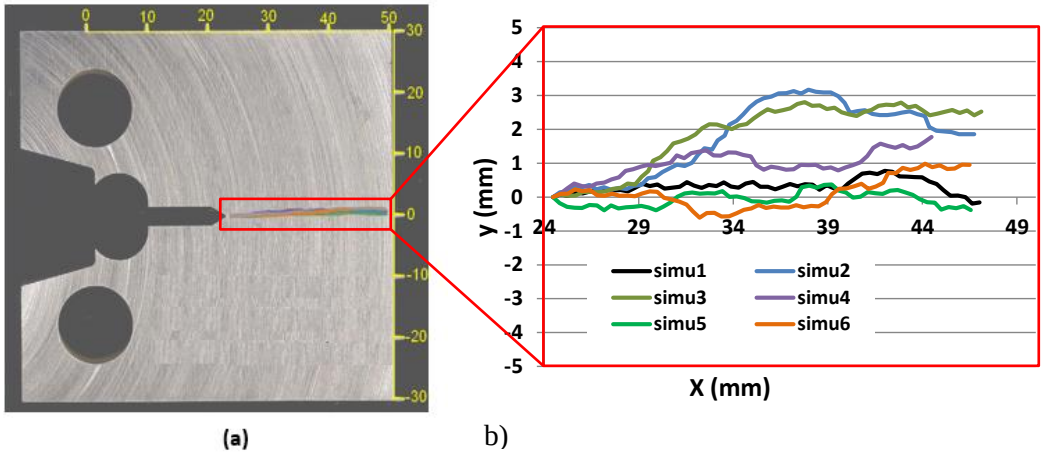

(a) b)

Figure 22: Predicted crack paths on standard CT25, obtained by using the probabilistic approach in the direction of crack propagation.

6 Conclusions

This paper presents an improved strain rate-dependent criterion to predict cleavage propagation and arrest in a PWR vessel steel (16MND5). This criterion, initially developed by Prabel [15] and Bousquet [17], is derived from Ritchie Knott and Rice model (RKR): the crack propagates as soon as the maximum principal stress σ_I reaches a critical value (σ_{IC}) at a given distance ($r_c = 100\mu m$) ahead of the crack tip. The critical stress (σ_{IC}) depends on the equivalent plastic strain rate ($\dot{\varepsilon}^p$), but not (or merely) on the temperature (at least in the range of investigated temperatures, and for the bainitic steel, used in this study).

The calculations are performed using eXtended Finite Element Method (X-FEM). The main elements of the numerical procedure and the criterion implementation are presented. The propagation criterion allows the determination the time increment related to a constant crack extension increment. A direction criterion based on the maximum hoop stress is used to define the direction of the crack extension.

In the first step of study, the criterion is identified by reproducing numerically 53 isothermal CT25 tests performed at four temperatures: -150°C, -125°C, -100°C and -75°C. Numerical results show that the critical stress (σ_{IC}) increases with the equivalent plastic strain rate ($\dot{\varepsilon}^p$), especially at high plastic stain rates. This is due to the effect of ductile ligaments acting as viscous back springs behind the crack tip.

The criterion is then applied to predict crack propagation and arrest on cracked rings submitted to a mixed mode loading (I+II) condition. The combination of the propagation criterion to a deterministic direction criterion provides a very good prediction in terms of the crack path, the crack growth rates and the location of the final crack arrest.

Extended CT specimens present a deflected path during propagation whereas the deterministic direction criterion predicts straight crack propagation. The observation of cross section by SEM on a standard CT25 reveals several secondary cracks on each side of the main crack. The observation of the crack extension in the beginning of propagation is carried out by using the high speed framing camera. It

shows that during the propagation the main crack joins one of the available micro-cracks presents ahead of the crack tip. From these observations, a probabilistic criterion is proposed to define the direction of crack propagation.

This probabilistic criterion is able to predict the crack deflection on the extended CT specimens and to predict the straight crack path on standard CT25 specimens as observed during the tests. Moreover, on the standard CT specimens, the shape of the predicted path presents local oscillations around the symmetry plane, which is closer to experimental path than that predicted by the deterministic criterion.

These results confirm the relevance of the propagation criterion proposed by Prabel [15, 16] and Bousquet [17] which was the first goal of this paper. The probabilistic criterion to predict the direction of crack extension proposed in this paper appears promising. However, complementary works are needed to consolidate the probabilistic criterion with a strongest link with micro-mechanical mechanisms involved in the cleavage fracture. Also, the application of this criterion on the precracked ring subjected to mixed mode loading will be a complementary action, before testing this criterion in the case of thermal shock.

7 Acknowledgements

The authors would like to thank T. Yurizinn, T. Le Grasse from the CEA/LISN team and CentraleSupélec Paris for their contributions to this work.

8 References

[1] ASTM E1221, 2010, “Standard Test Method for Determining Plane-Strain Crack Arrest Fracture Toughness, KIa, of Ferritic Steels”, ASTM Standard.

[2] Irwin G. R., Wells A. A., 1965, “A continuum mechanics view of crack propagation”, Metallurgical Review, Vol. 91, pp. 223-270.

[3] Dahl A 2012, “Etude experimental et approche locale de l’arret de fissure de clivage dans un acier bainitique”, PhD thesis, Ecole Centrale de Paris, France.

[4] Kalthoff J.F., 1977, “Mesurements of dynamic stress intensity factors for fast running and arresting cracks in double cantilever beam specimens”, ASTM STP 627, pp. 161–176.

[5] Kalthoff, J.F., Beinert J., Winkler S., Klemm W., 1980, “Experimental analysis of dynamic effects in different crack arrest test specimens”. ASTM STP 711, pp. 109–127.

[6] Hahn G.T., Hoagland R.G., Kanninen M.F., Rosenfield A.R., 1973, “A preliminary study of fast fracture and arrest in the DCB specimen”, Proc. Conf. Dynamic Crack Propagation, pp. 679-692.

[7] Kanninen M.F., Hudak S.J., Couque H.R., Dexter R.J., O'Donoghue P.E., 1990, “Viscoplastic-dynamic crack propagation: Experimental and analysis research for crack arrest applications in engineering structures”, International Journal of Fracture, Vol. 42, pp. 239-260.

[8] Ritchie R.O., Knott J.F., Rice J., 1973, “On the relationship between critical tensile stress and fracture stress in mild steels”, Journal of Mechanics and Physics of Solids, 21, pp. 395-410.

[9] Beremin F.M., Pineau A., Mudry F., Devaux J.-C., D’Escatha Y., Ledermann, P., 1983, “A local criterion for cleavage fracture of a nuclear pressure vessel steel”, Metallurgical and Materials Transactions A, 14, pp. 2277–2287.

[10] Iung T., Pineau A., 1996, “Dynamic crack propagation and crack arrest investigated with a new specimen geometry: Part II: Expériemental study study on low -alloy ferritic steel”, Fatigue and Fracture of Engineering Materials and Structures, 19, pp. 1369–1381.

[11] Bouyne E., 1999, “Propagation et arrêt de fissures de clivage dans l’acier 2 4/1 Cr-1 Mo”, PhD thesis, Ecole Nationale Supérieur des Mines de Paris, France.

[12] Hajjaj M., 2006, “Propagation et arret de fissure dans les cuves de reacteurs a eau pressurisee”, PhD thesis, Ecole Centrale de Paris, France.

[13] Dahl A., Berdin C., Moinereau D., 2011, “Dynamic Modeling of Cleavage Crack Propagation and Arrest with a Local Approach”, Procedia Engineering 10, pp. 1853–58.

[14] Berdin C., 2012, “3D modeling of cleavage crack arrest with a stress criterion”. Engineering Fracture Mechanics, 90, pp. 161–171.

[15] Prabel B., 2007, “Modelisation avec la methode X-FEM de la propagation dynamique et de l’arret de fissure de clivage dans un acier de cuve REP”, PhD thesis, INSA Lyon, France.

[16] Prabel B., Marie S., Combescure A., 2008, "Using the X-FEM Method to Model the Dynamic Propagation and Arrest of Cleavage Cracks in Ferritic Steel", Engineering Fracture Mechanics, 75, pp. 2984–3009.
[17] Bousquet A., 2013, "Propagation et arret de fissure un acier de cuve", PhD thesis, Ecole Centrale de Paris, France.
[18] Bousquet A., Marie S., Bompard P., 2012, "Cleavage Crack Propagation Characterization in a Nuclear Pressure Vessel Steel", Technische Mechanik, 32, pp. 118-129.
[19] Yang X., Marie S., Bompard P., Jacquemoud C., 2014, "Cleavage Crack Propagation and Arrest Prediction in French PWR Vessel Steel," Proc. ASME PVP conference, PVP2014-28422, Anaheim, US.
[20] Yang X., Jacquemoud C., Bompard P., Marie, S., 2015, "A Local Criterion to Predict Cleavage Crack Propagation and Arrest in a RPV Steel", Proc. 23th SMIRT conference, Manchester, UK.
[21] Chapuliot S., Lacire M.H., Marie S., Nédélec M., 2005, "Thermomechanical Analysis of Thermal Shock Fracture in the Brittle/ductile Transition Zone. Part I: Description of Tests", Engineering Fracture Mechanics, 72, pp. 661–673.
[22] Reytier M., Chapuliot S., Marie S., Ferry L., Nedelec M., 2006, "Study of Cleavage Initiation under Thermal Shock by Tests on Cracked Rings and Thermomechanical Calculations", Nuclear Engineering and Design, 236, pp. 1039–1050.
[23] Yang X., 2015, "Prediction de la propagation et de l'arrêt de fissure de clivage dans un acier de cuve REP (16MND5) sous choc thermique", PhD thesis, Ecole Centrale de Paris, France.
[24] Cast3M, 2017, http://www-cast3m.cea.fr.
[25] Reytier M., Chapuliot S., Marie S., Nedelec M., 2006, "Thermomechanical analysis of thermal shock fracture in the brittle/ductile transition zone—Part II: Numerical calculations and interpretation of the test results", Engineering Fracture Mechanics, 73, pp. 283–295.
[26] Prabel B., Combescure A., Marie, S., 2007, "Dynamic crack propagation in elastic-plastic media with Xfem", International Journal for Numerical Methods in Engineering, 69, pp.1553-1569.
[27] Sumi, Y., 1985, "Computational crack path prediction", Theoretical Applied Fracture Mechanics, 4, pp. 149–156.
[28] Chen B., Dillard D.A., 2001, "The effect of the T-stress on crack path selection in a adhesively bonded joints", International Journal of Adhesion and Adhesives, 21, pp. 357-368.
[29] Becker T.L. Jr., Cannon R. M., Ritchie R.O., 2001, "Finite crack kinking and T-stresses in functionally graded materials", International Journal of Solids and Structures, 38, pp. 5545-5563.
[30] Jablokov V., Goto D.M., Koss D.A., McKirgan, J.B, 2001, "Temperature, strain rate, stress state and the failure of HY-100 steel". Materials Science and Engineering, A 302, pp. 197–205.
[31] Chapuliot S., Le Corre V, 2008, "A simplified expression for low cleavage probability calculation", Engineering Fracture Mechanics, 75, pp. 1488–1506.
[32] Miannay D., 1998, Fracture Mechanics, Mechanical Engineering Series, Springer.
[33] Berdin C., Hajjaj M., Bompard P., Bugat S., 2008, "Local Approach to Fracture for Crack Arrest Prediction", Engineering Fracture Mechanics, 75, pp. 3264-3275.
[34] Hausild P., Berdin C., Bompard P., 2005, "Prediction of cleavage fracture for a low-alloy steel in the ductile-to-brittle transition temperature range", Materials Science and Engineering, A, 391, pp. 188-197.
[35] Leguillon D., Murer S., 2008, "Crack deflection in a biaxial stress state", International Journal of Fracture, 150, pp. 75-90.
[36] Sapora A., Cornetti P., Mantic V., 2016, "T stress effects on crack deflection: Straight vs curved crack advance", European Journal of Mechanics A/Solids, 60, pp. 52-57.
[37] Bousquet A., Marie S., Bompard P., 2012, "Cleavage crack propagation and arrest in a nuclear pressure vessel steel", Proc. ASME PVP conference, PVP2012-78174, Toronto, Canada.
[38] Bousquet A., Marie S., Bompard P., 2012, "Cleavage dynamic propagation analysis in a nuclar reactor pressure vessel steel using a high-speed camera", Proc. ASME PVP conference, PVP2012-78169, Toronto, Canada.
[39] Elguedj T., Gravouil A., Combescure A., 2006, "Appropriate extended functions for XFEM simulation of plastic fracture mechanics". Computer Methods in Applied Mechanics and Engineering, 195, pp. 501–515.

[40] Newmark NM., 1959, “A method of computation for structural dynamics”, Proc. ASCE, 85, pp. 67–94.
[41] Sumi Y., Mu Y., 2000, “Thermally induced quasi-static wavy crack propagation in a brittle solid, Mechanics of Materials”, 32, pp. 531-542.